Supporting information

Enhancing the Coupling Effect in Sandwiched $FeNiPS_3$/Graphite Catalyst Derived from Graphite Intercalation Compounds for Efficient Oxygen Evolution Reaction

Licheng Wei [1], Song Huang [1], Yufei Zhang* [1, 2], Minghui Ye [1], Cheng Chao Li* [1, 2]

1 School of Chemical Engineering and Light Industry, Guangdong University of Technology, Guangzhou 510006, China.

2 Guangdong Provincial Key Laboratory of Plant Resource Biorefinery, Guangzhou, 510006, China.

Corresponding Authors at: School of Chemical Engineering and Light Industry, Guangdong University of Technology, Guangzhou 510006, China (C. Li).

*E-mail addresses: licc@gdut.edu.cn (C. Li)

Experimental section

Anhydrous Ferric chloride ($FeCl_3$), anhydrous nickel chloride ($NiCl_2$) and potassium hydroxide (KOH) were purchased from Mclean Chemical Reagent Co., Ltd. Graphite powder with 1200 mesh and sulfur powder was purchased from Aladdin Chemical Reagent Co., Ltd. Phosphorus powder was purchased from Tianjin Damao Chemical Reagent Factory. Nafion (5wt%) was purchased from Sigma-Aldrich.

Synthetic Method

Firstly, $FeCl_3$ and $NiCl_2$ with proportion of 7:3 were inserted into graphite layers by molten-salt method at 400 ℃ for 24 h in vacuum for obtaining the first-order graphite intercalation compounds ($FeCl_3$-$NiCl_2$-GIC).[1] Secondly, the prepared first-order $FeCl_3$-$NiCl_2$-GIC was evenly ground with phosphorus powder and sulfur powder according to the molar ratio of 1:1:3, and further sealed into a vacuum quartz tube. Finally, the $FeNiPS_3$ sandwiched graphite layers composites ($FeNiPS_3$/GL) were obtained by solid-state reaction at 550 ℃ for 30 minutes under vacuum condition. For comparison, pure carbon reacted with phosphorus powder and sulfur powder under the same condition to prepare P and S co-doping carbon (C-PS). Similarly, the $FePS_3$ sandwiched with graphite layers ($FePS_3$/GL) was prepared by transforming $FeCl_3$-GIC. Other $FeNiPS_3$/GLs with adding $FeCl_3$ and $NiCl_2$ proportions of 10:0, 9:1, 8:2 were also prepared for comparison and marked as $FePS_3$/GL, $FeNiPS_3$/GL-91 and $FeNiPS_3$/GL-82, respectively. And the pure $FePS_3$ was prepared by reacting iron powder, phosphorus powder and sulfur powder for 12 h.

Physical characterization

XRD patterns were tested by Rigaku SmartLab polycrystall X-ray diffraction with Cu Kα radiation (λ=1.54 Å). Raman spectra of the samples were recorded on HORIBA Jobin Yvon LabRAM HR800 UV Laser Raman Spectroscopy. FTIR spectra were collected by a FTIR spectrometer (Nicolet iS5, Thermo Scientific). The morphology characterization was achieved by scanning electron microscopy (SEM, SU8220) and transmission electron microscopy (TEM, FEI Tecnai G2 F30). XPS spectra were tested on X-ray photoelectron spectroscopy (XPS, Escalab 250Xi). The thickness of sample was characterized by Dimension Fast Scan.

Electrochemical characterization

Electrochemical measurements were performed on PINE-WaveDriver100 and Gamry electrochemical workstation with classic three-electrode system with working electrode of glassy carbon electrode (diameter: 5 mm) coating with catalytic ink, reference electrode of Hg/HgO electrode and counter electrode of graphite rod in 1.0 M KOH situation. Working electrode was prepared by dropping catalyst ink on the surface of glassy carbon disk with loading catalyst mass of 0.1 mg. The catalyst ink is prepared by dispersing 5 mg catalyst in solution with 490 μL ethanol and Nafion (10 μL, 5 wt%) and ultrasonication for 1 h. The polarization curves of OER test were performed in 1.0 M KOH electrolyte at scan rate of 5 mV s^{-1}. Electrochemical Impedance Spectroscopy (EIS) was measured at 1.50 V during the frequency range of 1×10^{5}-1×10^{-1} Hz. The durability of the samples was characterized by

chronopotentiometry. The potentials of OER tests are converted to the reversible hydrogen electrode (RHE) based on Nernst equation. All potential in this work was calculated without IR compensation, unless special explain.

$$E_{RHE}=E_{Hg/HgO}+0.098+0.059PH \quad (1)$$

Tafel slope can be calculated by following equation:

$$\eta = a+b\log j \quad (2)$$

Where η represents the overpotential and j is the current density.

The electrochemically active surface area (ECSA) is positive relating with double layer capacitance (C_{dl}) that can be calculated by following:

$$ECSA=C_{dl}/Cs \quad (3)$$

Here, Cs represents a general specific capacitance of 0.040 mF cm^{-2} in 1.0 M KOH solution. C_{dl} is calculated according to cyclic voltammograms cycles (CVs) with scan rates of 100, 200, 300, 400 and 500 mV s^{-1}.

Besides, turnover frequency (TOF) measures by the following relation:

$$n\ (mol)=Q/4F \quad (4)$$

$$TOF\ (s^{-1})=I/4nF \quad (5)$$

n represents the number of active sites calculated by the CVs under the potential range from 0.9-1.7 V (vs. RHE) at 50 mV s^{-1} in 1.0 M PBS electrolyte (PH = 7.0). Q is voltammetric charges that are calculated by the differential capacitance of CV curves. F represents Faraday's constant of 96,485 C mol^{-1}. I (A) belong to the current of the polarization curve measured by LSV.

The oxygen gas was analyzed by online gas chromatography (GC) at different times.

O_2 was quantified by a thermal conductivity detector (TCD). Calculation of the Faradaic efficiency of O_2:

$$fgas = \frac{f_{flow} \times c_{gas} / V_m \times n \times F}{I \times 60} \times 100 \quad (6)$$

f_{gas}: Faradaic efficiency of O_2, %;

f_{flow}: flow rate of O_2, mL min^{-1};

I: electrolysis current, A;

c_{gas}: volume ratio of gas product, determined by online GC;

V_m: the molar volume of an ideal gas at 1 atmosphere of pressure, 22400 mL mol^{-1};

n: number of transferred electrons for certain product;

F: Faraday's constant, 96485 C mol^{-1}.

The zinc air battery was assembled with zinc plate anode, air cathode and alkaline electrolyte (6.0 M KOH electrolyte solution including 0.2 M $Zn(OAc)_2$). The catalyst layer on air cathode was fabricated by dropping the catalyst ink on carbon clothes, which catalyst loading mass of 2.0 mg cm^{-2}. The long-term galvanostatic charge and discharge for zinc air battery was measured on Neware Battery Charge and Discharge Test System was set at a cycling period of 20 min at current density of 5 mA cm^{-2}.

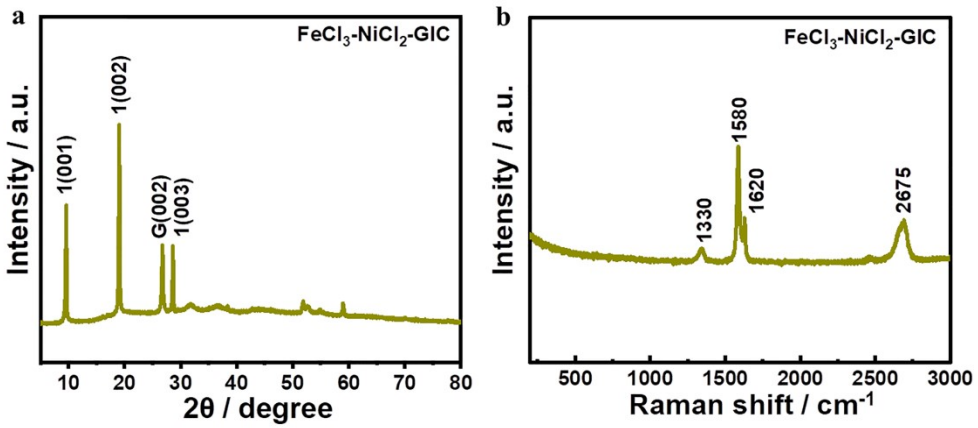

Fig. S1. (a) XRD pattern and (b) Raman spectrum of $FeCl_3$-$NiCl_2$-GIC-73.

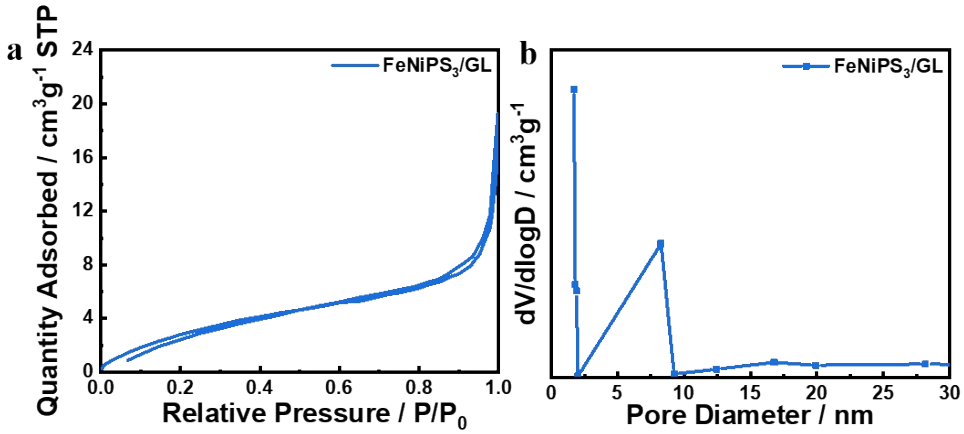

Fig. S2. (a) N_2 absorption-desorption isotherms and (b) pores distribution of $FeNiPS_3$/GL.

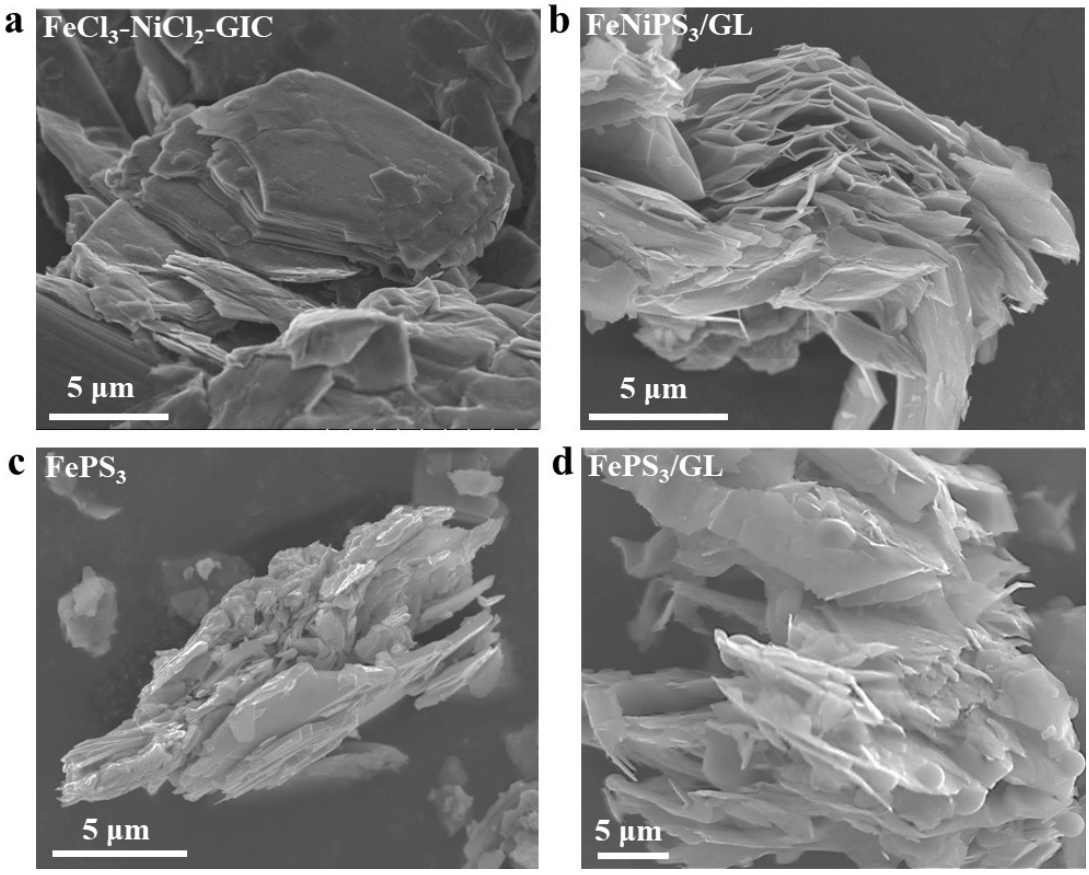

Fig. S3. SEM images of (a) $FeCl_3$-$NiCl_2$-GIC, (b) $FeNiPS_3$/GL, (c) $FePS_3$ and (d) $FePS_3$/GL.

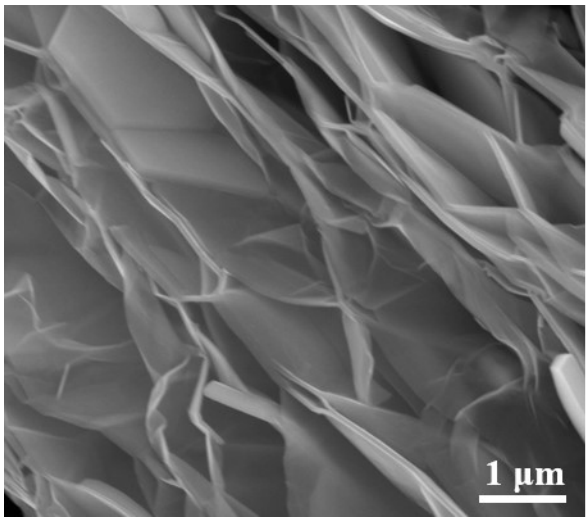

Fig. S4. High-resolution SEM image of $FePS_3$/GL.

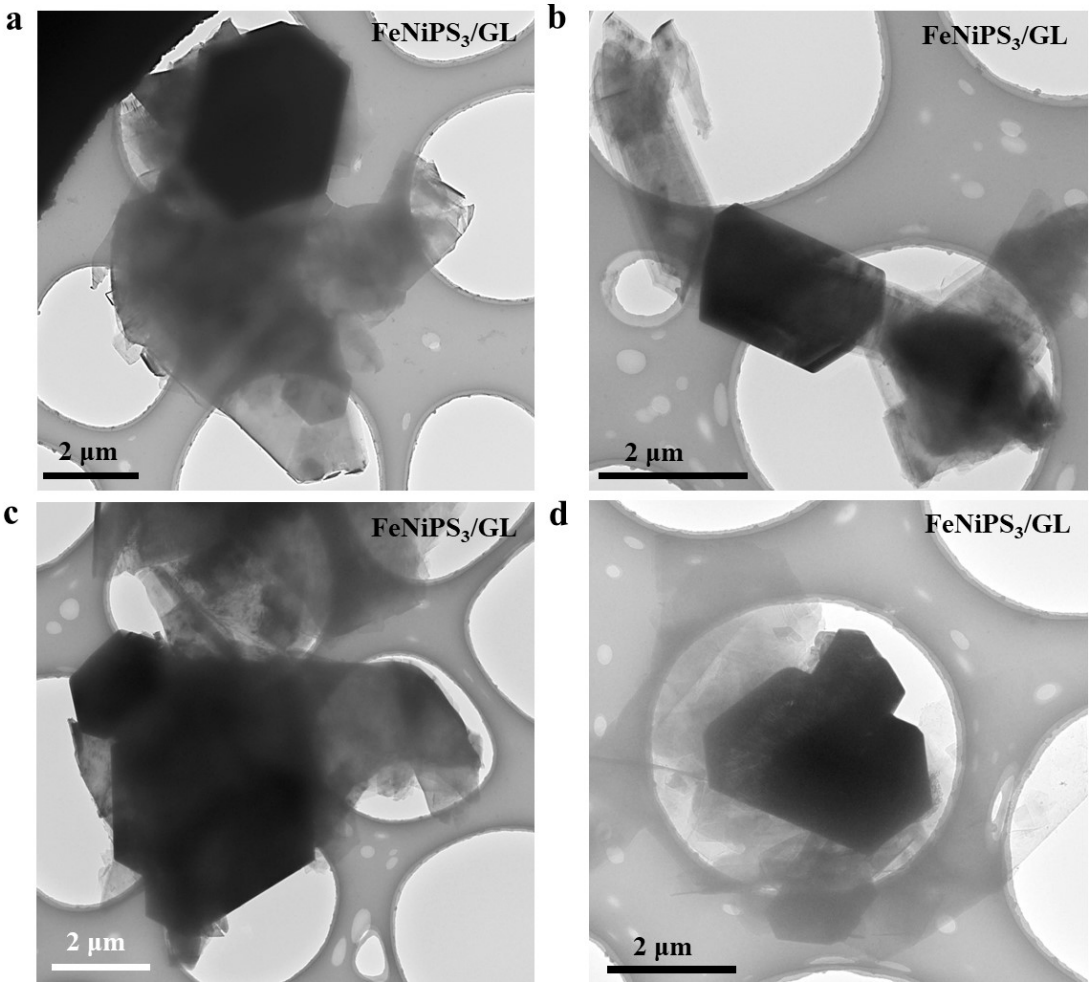

Fig. S5. (a-d) Low-resolution TEM images of $FeNiPS_3$/GL.

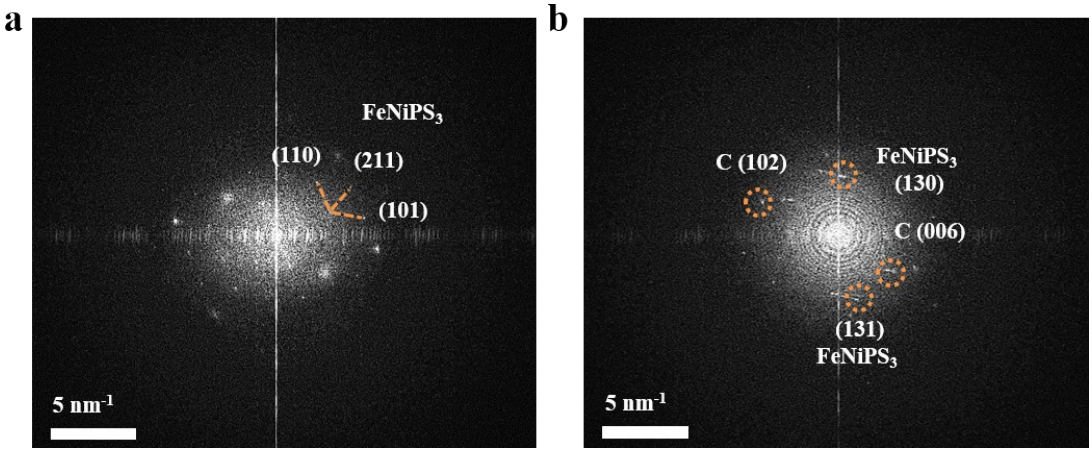

Fig. S6. (a-b) FFT images transforming from high-resolution TEM images of $FeNiPS_3$/GL.

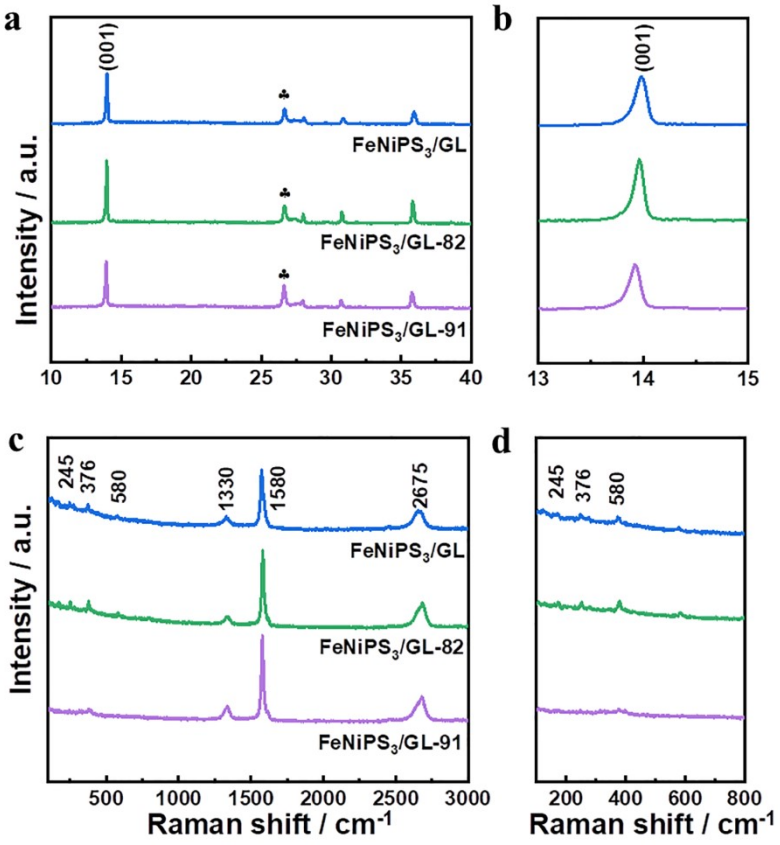

Fig. S7. (a-b) XRD patterns and (c-d) Raman spectra of $FeNiPS_3$/GL-91/82 and $FeNiPS_3$/GL.

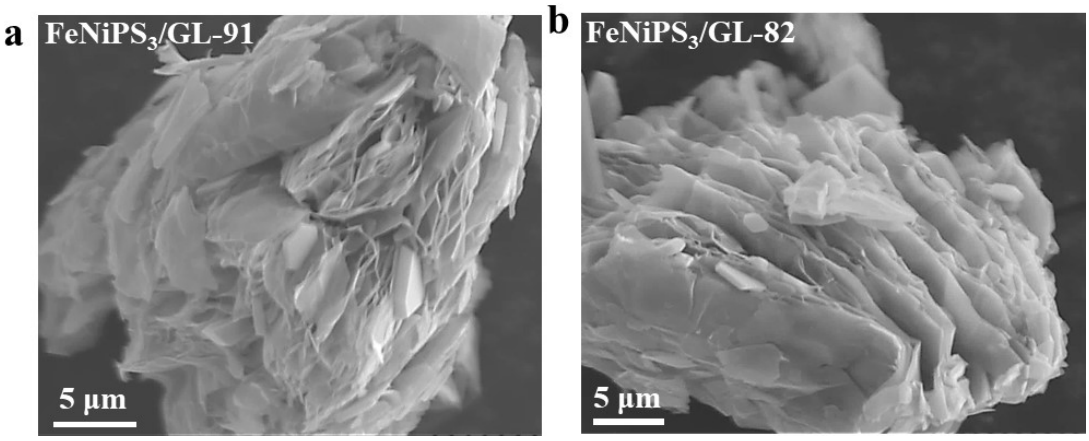

Fig. S8. SEM images of (a) $FeNiPS_3$/GL-91, (b) $FeNiPS_3$/GL-82.

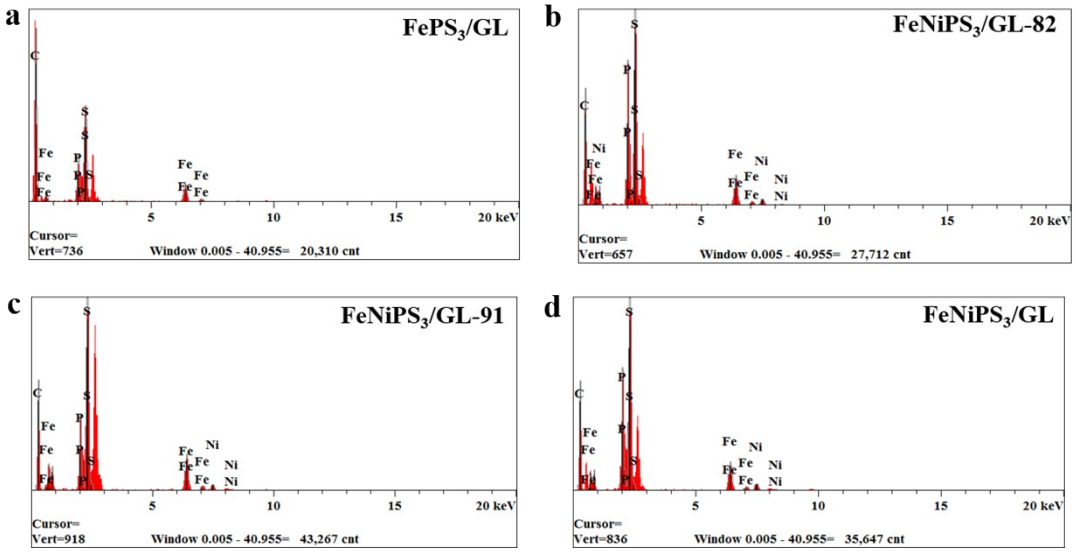

Fig. 9. (a-d) the EDS spectra of series $FePS_3$/GL and $FeNiPS_3$/GLs.

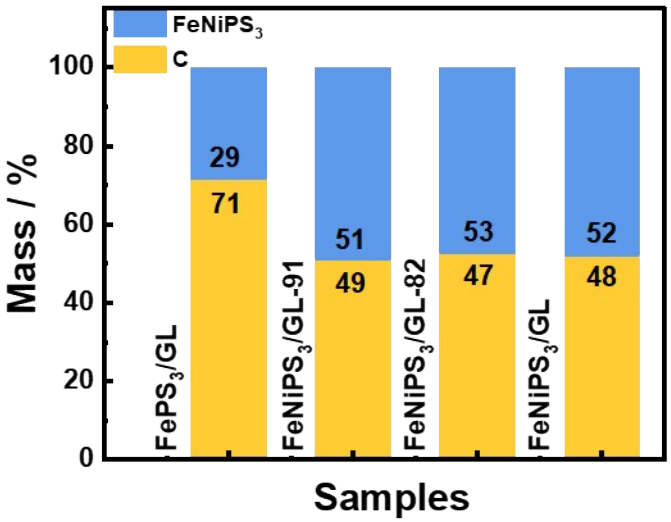

Fig. S10. Bar chart of different mass ratios of graphite and $FePS_3$ or $FeNiPS_3$.

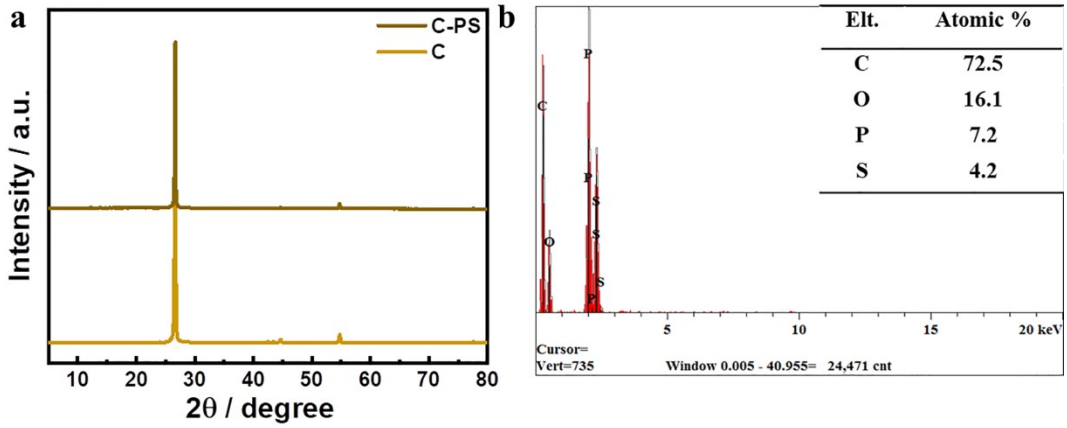

Fig. S11. (a) The XRD patterns of C and C-PS. (b) The EDS spectrum of C-PS.

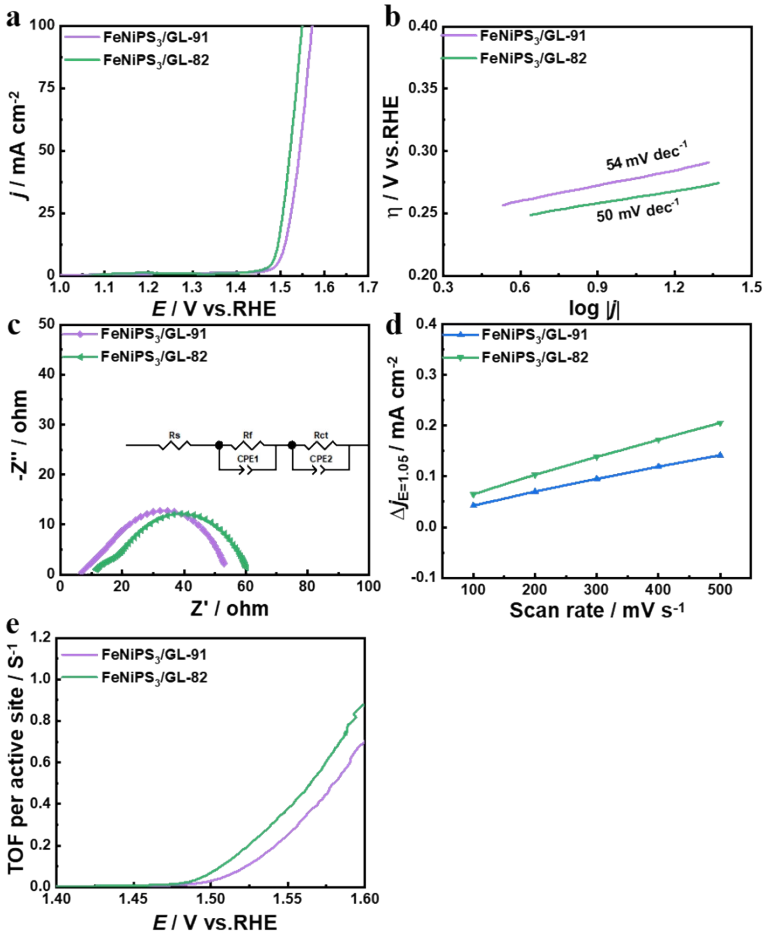

Fig. S12. (a) Polarization curves of $FeNiPS_3$/GL-91/82. (b) Corresponding Tafel slope. (c) Nyquist plots (inset: inset: equivalent circuit). (d) Capacitive current related with scan rates from 100 to 500 mV s^{-1}. (e) TOF values at different fixed overpotentials.

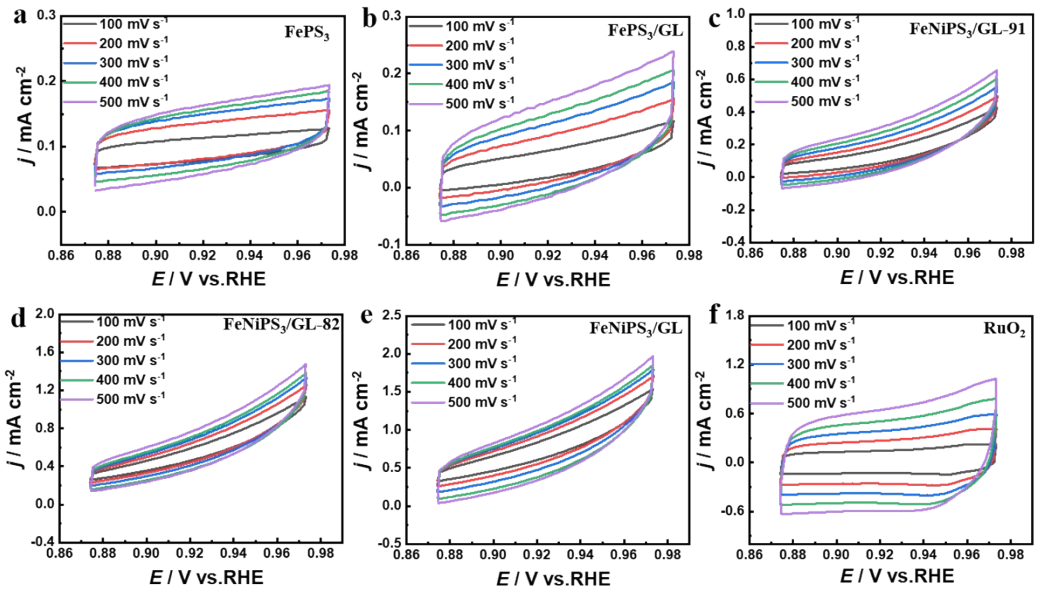

Fig. S13. CV curves of $FePS_3$, $FePS_3$/GL, $FeNiPS_3$/GL-91, $FeNiPS_3$/GL-82, $FeNiPS_3$/GL and RuO_2.

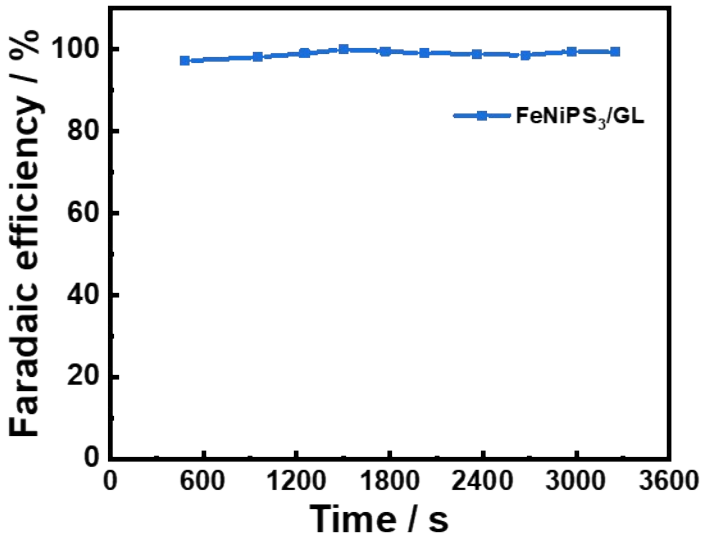

Fig. S14. The Faradaic efficiency of $FeNiPS_3$/GL calculated by online gas chromatography.

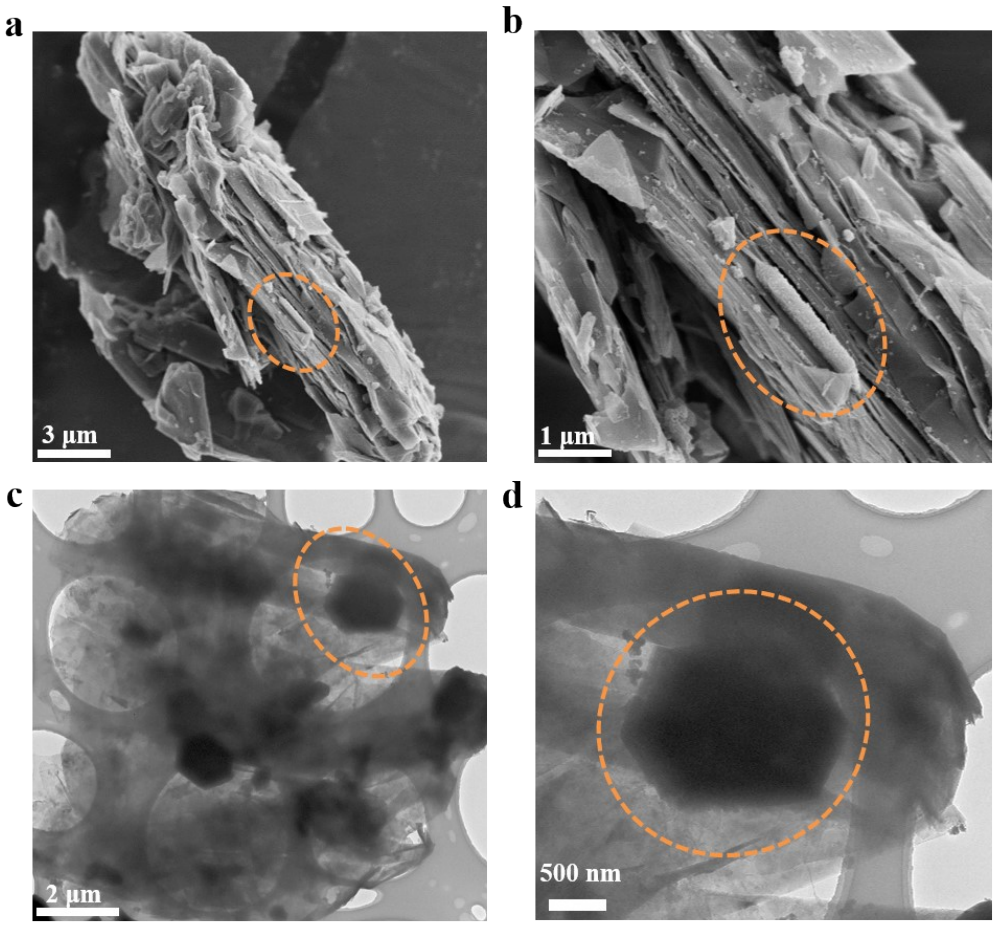

Fig. S15. (a-b) SEM images and (c-d) TEM images of $FeNiPS_3$/GL after 100 h test.

Table S1. The atom ratios of Fe and Ni in various GICs tested by EDS.

	C	Cl	O	Fe	Ni
$FeCl_3$-GIC	72.84	18.42	0.85	7.89	-
$FeCl_3$-$NiCl_2$-GIC-91	70.14	18.12	4.42	6.36	0.96
$FeCl_3$-$NiCl_2$-GIC-82	65.80	15.16	9.31	7.83	1.90
$FeCl_3$-$NiCl_2$-GIC-73	65.77	14.00	11.80	5.80	2.62

Table S2 The ICP result of $FePS_3$/GL and $FeNiPS_3$/GLs.

ICP-MS μg L^{-1}	**Ni**	**Fe**
$FePS_3$/GL	0.785	97.961
$FeNiPS_3$/GL-91	25.887	90.968
$FeNiPS_3$/GL-82	42.456	62.730
$FeNiPS_3$/GL-73	50.201	67.625

References

1. M. Inagaki, Z. D. Wang, Y. Okamoto and M. Ohira, *Synth. Met.*, 1987, **20**, 9-13.